Chin. J. Astron. Astrophys. Vol. 6 (2006), No. 6, 705–715
(*http://www.chjaa.org*)

Chinese Journal of
Astronomy and
Astrophysics

Chaos in Compact Binaries with Frequency Map Analysis *

Yi Xie and Tian-Yi Huang

Department of Astronomy, Nanjing University, Nanjing 210093; *yi.s.xie@gmail.com*

Received 2006 March 31; accepted 2006 June 27

Abstract The dynamics of compact binaries is very complicated because of spin-orbit coupling and spin-spin coupling. With Laskar's frequency map analysis (FMA) and frequency diffusion as an indicator, we found that misalignment of the spins and orbital angular momentum has a great effect on the dynamics, and for systems with different mass ratios $\beta \equiv m_2/m_1$ chaos occurs at different spin-orbit configurations. For equal-mass binaries ($\beta = 1$), chaos occurs when the spins nearly cancel each other out. For some other systems (for example $\beta \sim 1/2$), the binaries are irregular, even chaotic, when the spins are perpendicular to the orbital angular momentum. For the case where gravitational radiation is taken into account, we give an analytic estimation for the frequency diffusion based on the decay of the orbit, which is roughly consistent with our simulations. This means the FMA is not suitable as a chaos indicator for weak chaotic cases with dissipative terms.

Key words: celestial mechanics — (stars:) binaries (including multiple): close

1 INTRODUCTION

Owning to the high nonlinearity of Einstein's field equation, chaos will occur naturally. Several authors have found chaos in several relativistic systems (Varvoglis & Papadopoulos 1992; Karas & Vokrouhlicky 1992; Bombelli & Calzetta 1992; Dettmann et al. 1994; Wu et al. 2006; Wu & Zhang 2006). However, those systems are idealized. In the cases of astrophysics, chaos in compact binaries is much more meaningful.

Compact binaries, including black hole – black hole, neutron star - black hole and neutron star – neutron star systems, are important sources of gravitational waves for ground-based observatories, such as LIGO, VIRGO and GEO600. However, chaos could make the number of templates that matches the observed waveform increase exponentially, rendering impractical template-based gravitational wave detection. Furthermore, a binary with a pulsar is an ideal lab for checking general relativity in strong field by radio observation on the time of arrival of pulses, especially for the Square Kilometre Array (SKA, Kramer 2004).

According to the mass ratio $\beta \equiv m_2/m_1$, binaries can be classified as (1) extreme mass ratio binaries ($\beta \ll 1$) and (2) comparable-mass binaries ($\beta \sim 1$), and they are described by different models in the frame of general relativity. Several authors have studied their dynamical behavior, and obtained some results.

An example of extreme mass ratio binary is one where one component is a supermassive black hole ($\sim 10^6 M_\odot$) in a galactic nucleus and the other component is a stellar-sized compact star ($\sim 1 - 10 M_\odot$). Suzuki & Maeda (1997) studied the motion of a spinning particle in Schwarzschild spacetime with Lyapunov characteristic exponent (LCE) and Poincaré section. They found that the motion of the particle can be chaotic under some appropriate conditions, which is purely induced by the spin-orbit interaction. However, their chaotic conditions of spin are unphysical [1]. Later, Hartl (2003a,b) investigated the dynamics of spinning test particles in Kerr spacetime, and found that, for all physically realistic values of spin, chaos does not happen, and that in principle there is no chaos in extreme mass ratio binaries.

∗ Supported by the National Natural Science Foundation of China.

[1] A dimensionless spin parameter $S = s/(mM)$ is usually defined in a binary system with component masses m and M, where s is the spin angular momentum of the component m and the $c = 1, G = 1$ unit system is adopted. For an extreme Kerr black hole $s = m^2$, then $S = m/M$. Consequently, for an extreme mass ratio binary we have $S \ll 1$. The value adopted by Suzuki & Maeda (1997) is $S \sim 1$, which should be considered as unphysical. However, for a comparable mass ratio binary, S can reach 1 maximally.

The case of comparable-mass compact binaries is more complicated. Different authors have obtained different results. Levin (2000) investigated spinning compact binaries, using fractal basin boundary scan as a chaos indicator, and found some fractal structures in the survey, which mean chaos. Soon after that, Schnittman & Rasio (2001) reexamined Levin's result and found no chaotic behavior by LCE, and placed a lower limit on the divergence time that is many times greater than one typical inspiral time. As a response, Cornish & Levin (2003) stated that, by using LCE, they did find that some eccentric orbits to have chaotic behavior but the chaos is damped by dissipation so that most orbits will only be mildly affected.

In addition, Levin (2003) studied chaotic initial conditions in comparable-mass compact binaries in detail for two values of mass ratios, $1.4/10$ and $1/3$. She found that the transition to chaos occurs as the sizes of the spin and the misalignment are increased, which is consistent with her previous result that some orbits will remain regular as a circular inspiral with the spins exactly aligned with the orbital momentum (Levin 2000). Hartl & Buonanno (2005) claimed that there is no chaos in physical cases. Using LCE, they surveyed different mass configurations: $(20{+}25)M_\odot$, $(10{+}5)M_\odot$, $(5{+}5)M_\odot$, $(10{+}10)M_\odot$, $(20{+}20)M_\odot$, $(20+10)M_\odot$, and $(10+5)M_\odot$, at a gravitational wave frequency $f_{\rm GW}^{\rm Newt} = 240$ Hz quasicircular orbit with 500 randomly oriented initial spins for each case. It was found that chaotic orbits only occur for the $(10{+}10)M_\odot$ (fraction 0.002) and $(20{+}10)M_\odot$ (fraction 0.104) mass configurations. For $(10{+}10)M_\odot$, the chaotic orbits are clustered at the lowest values of the total angular momentum J, corresponding to initial spin vectors nearly antiparallel to the orbital angular momentum $\boldsymbol{L}$ (so that $J = |\boldsymbol{L} + \boldsymbol{S}|$ is minimized). Chaos for the $(20 + 10)M_\odot$ configuration occurs mainly for values of J in the middle of the possible range. In all eccentric cases considered, they found no evidence of chaos. However, we wonder why there is no chaos in the case of $(20 + 20)M_\odot$ for which the relativistic correction is larger than for the case of $(10 + 10)M_\odot$.

An important difference in the dynamics between relativistic and Newtonian systems is the chaos indicator. In Newtonian dynamics, chaos emerges when nearby trajectories separate exponentially in a compact phase space, which could be indicated by the LCE,

$$\lambda_i = \lim_{t\to\infty} \frac{\log[\Delta r_i(t)]}{t}. \tag{1}$$

Whereas, for relativistic systems there exists ambiguity in the meaning of space and time coordinates in the sense of measurement, which can be chosen arbitrarily. Consequently, an LCE defined in Newtonian mechanics would be not applicable in general relativity and a covariant Lyapunov exponent should be used, such as Wu & Huang (2006a). Now, Suzuki & Maeda (1997) and Hartl (2003a,b) did not use a strict covariant Lyapunov exponent. In the survey of Hartl (2003a, b), but used an unrenormalized deviation vector method to calculate the LCE because of its speed. That is not a robust method. Besides, fractal basin boundary scan was used, because of its independence of the coordinate system, as in Levin (2000, 2003).

In this paper, the chaos indicator we use is Laskar's FMA (Frequency Map Analysis) and frequency diffusion. A dynamical system generates a time series and periodic orbits correspond to constant line peaks in the frequency map and power spectrum. Quasiperiodic orbits correspond to peaks of finite widths, and shifting in time. For chaotic orbits, the power spectrum has no line peaks and is a continuum. Unfortunately, owning to the poor precision in extracting frequencies by the widely used fast Fourier transform (FFT), it is difficult to distinguish complicated regular, quasiperiodic and weak chaotic orbits, but Laskar's scheme overcomes this problem (see Sec. 3 below for details of its implementation and its validity for compact binaries).

The arrangement of this paper is as follows. Section 2 shows the equations of motion of orbit and spin and the conservation laws in compact binaries. Section 3 presents a brief introduction to Laskar's FMA. In Section 4 we give the results from our numerical simulations.

2 THE EQUATIONS OF MOTION OF ORBIT AND SPIN

To use full relativistic solution for compact binaries would be a formidable job so we adopt the post-Newtonian (PN) expansion for relativistic 2-body problem (Kidder 1995). This includes the equations of motion up to 2 PN ($O(c^{-4})$), 2.5 PN gravitational radiation term and spin equations with de Sitter and Lense-Thirring precession (Bark & O'Connell 1975). Although the post-Newtonian converges slowly, especially when the gravitational field is strong, it could still give a qualitative picture of compact binaries, such as the nonlinear effects, the existence of unstable circular orbits and the nature of spin precession.

With harmonic gauge, the PN expansion of the equation of orbital motion is (Kidder 1995)

$$\ddot{\boldsymbol{r}} = \boldsymbol{a}_N^{(0)} + \boldsymbol{a}_{\rm PN}^{(1)} + \boldsymbol{a}_{\rm SO}^{(1.5)} + \boldsymbol{a}_{\rm PN}^{(2)} + \boldsymbol{a}_{\rm SS}^{(2)} + \boldsymbol{a}_{\rm RR}^{(2.5)} + \cdots , \tag{2}$$

where $\boldsymbol{a}_{\rm N}^{(0)}$ is the Newtonian term, $\boldsymbol{a}_{\rm PN}^{(1)}$ the first order PN acceleration, which induces the precession of periastron, $\boldsymbol{a}_{\rm PN}^{(2)}$ is the second order PN acceleration, which induces the innermost stable circular orbit. The spin-orbit coupling term $\boldsymbol{a}_{\rm SO}^{(1.5)}$ and spin-spin coupling term $\boldsymbol{a}_{\rm SS}^{(2)}$ cause the orbital angular momentum to precess, $\boldsymbol{a}_{\rm RR}^{(2.5)}$ is the reaction term of gravitational radiation, which is a dissipative term in PN expansion and causes the energy and orbital angular momentum to decay.

The spin equation is (Barker & O'Connell 1975)

$$\dot{\boldsymbol{S}}_i = \boldsymbol{\Omega}_i \times \boldsymbol{S}_i \,, \qquad i = 1, 2, \tag{3}$$

where

$$\boldsymbol{\Omega}_i = \boldsymbol{\Omega}_{i_{\rm dS}} + \boldsymbol{\Omega}_{i_{\rm LT}} \,, \qquad i = 1, 2, \tag{4}$$

in which $\boldsymbol{\Omega}_{i_{\rm dS}}$ is the de Sitter precession and $\boldsymbol{\Omega}_{i_{\rm LT}}$ is the Lense-Thirring precession.

If the gravitational radiation is neglected, the total energy E and total angular momentum $\boldsymbol{J} = \boldsymbol{L} + \boldsymbol{S}$ are conservative up to 2 PN and 1.5 PN, respectively, which are

$$E = E_{\rm N} + E_{1\,\rm PN} + E_{2\,\rm PN} + E_{\rm SO} + E_{\rm SS}, \tag{5}$$

$$\boldsymbol{L} = \boldsymbol{L}_{\rm N} + \boldsymbol{L}_{1\,\rm PN} + \boldsymbol{L}_{2\,\rm PN} + \boldsymbol{L}_{\rm SO}, \tag{6}$$

$$\boldsymbol{S} = \boldsymbol{S}_1 + \boldsymbol{S}_2. \tag{7}$$

3 FREQUENCY MAP ANALYSIS

In the early 1990's, Laskar proposed the method of FMA (Laskar 1990, 1993) for investigating dynamical systems. In the application of the standard map, it was shown that the FMA is even sensitive to weak chaos (Laskar et al. 1992). Here we give a brief introduction to this method which heavily depends on observation. For a time series $f(t)$ defined in $\mathbb{C}$, one could construct a quasiperiodic approximation of $f(t)$ in the time interval $[-T, T]$, which converges to $f(t)$ when T tends to infinity.

Assume that

$$f(t) = e^{i\nu_1 t} + \sum_{k \in \mathbb{Z}^n - (1,0,\ldots,0)} a_k e^{i\langle k,\nu\rangle t}, \qquad a_k \in \mathbb{C} \tag{8}$$

in which the frequency vector (ν) satisfies the Diophantine condition. Laskar proposed an iterative algorithm to find approximate values of all the frequencies and their corresponding amplitudes. First, a scalar product is defined as

$$\langle f(t), g(t)\rangle = \frac{1}{2T}\int_{-T}^{T} f(t)\overline{g}(t)\chi(t)dt, \tag{9}$$

where $\chi(t)$ is a positive, even weight function and $\overline{g}(t)$ is the complex conjugate of $g(t)$. With the weight function $\chi(t) = \chi_p(t)$,

$$\chi_p(t) = \frac{2^p(p\,!)^2}{(2p)!}(1 + \cos\pi t)^p, \tag{10}$$

in the time interval $[-T, T]$, the algorithm of FMA could obtain ν_1^T, an approximation of ν_1, by requiring that $\langle f(t), e^{i\nu_1^T t}\rangle$ reaches maximum. As $T \to \infty$, ν_1^T converges to ν_1. Their difference is

$$\nu_1 - \nu_1^T = \frac{(-1)^{p+1}\pi^{2p}(p\,!)^2}{A_p T^{2p+2}} \sum_k \frac{\Re(a_k)}{\Omega_k^{2p+1}} \cos(\Omega_k T) + O\Big(\frac{1}{T^{2p+2}}\Big), \tag{11}$$

where $\Omega_k = \langle k, \nu\rangle - \nu_1$, $A_p = -2(\pi^2/6 - \sum_{k=1}^{p} 1/k^2)/\pi^2$. Especially, with $p = 1$, the accuracy of ν_1^T we obtained is proportional to $1/T^4$, as compared to $1/T$ with the FFT. Therefore, $(\nu_1, \nu_2, \ldots, \nu_n)$ could

be determined one by one precisely with FMA. The PN expansion of the equations of motion satisfies the assumption of FMA.

To apply FMA to compact binaries, we define a complex function $f_o(t)$ for their orbital motion as

$$f_o(t) = |\boldsymbol{r}| \sin\theta e^{i\varphi}, \tag{12}$$

where θ and φ are the Euler angles (see Fig. 1).

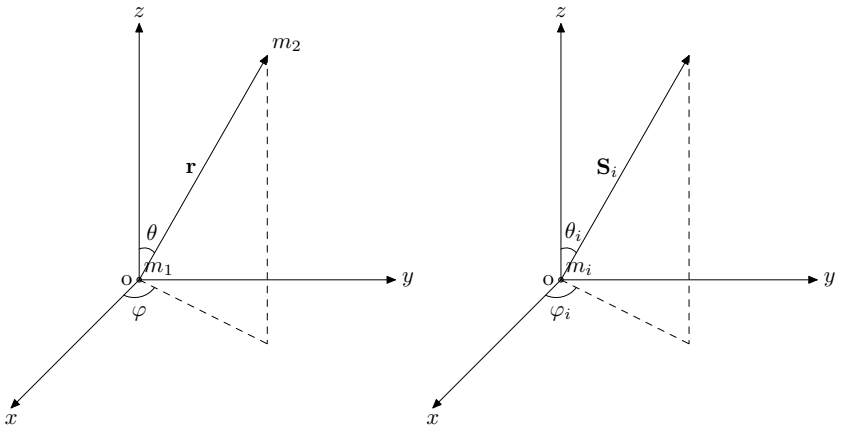

Fig. 1 Left: $\boldsymbol{r}$ is the vector connecting two stars and φ and θ are its Euler angles. Right: $\boldsymbol{S}_i$ is one of the spins, φ_i and θ_i are its Euler angles, where $i = 1, 2$. See text for the adopted coordinate system.

In addition, we define the frequency diffusion σ after Robutel & Laskar (2000), which is an indicator of chaos, as

$$\sigma = 1 - \frac{\nu_2}{\nu_1}, \tag{13}$$

where ν_1 and ν_2 are the fundamental frequencies obtained in the time intervals $[0, T]$ and $[T, 2T]$, respectively.

4 NUMERICAL RESULTS

In our numerical simulations, the coordinate system we adopted is a Cartesian coordinate system o-xyz, with origin at one of the compact stars, m_1, and the plane xy and the x axis respectively the orbital plane and the line connecting the two components at the initial instant. With PN expansion, this system can be taken as a system close to being integrable, in which Gm/c^2r or v^2/c^2 are small parameters, ($m = m_1 + m_2$). The spins of the compact stars are $S_i = \chi_i G m_i^2/c$, in which χ_i is the spin parameter and $\chi_i \leqslant 1$. The initial orientations of the spins are $\varphi_1 = \varphi_2 = 0$ and θ_1 and θ_2 are left as free parameters. Hereinafter, we use $G = 1$ and $c = 1$ units, and in Section 4.1 and 4.2, we will check only the cases of quasicircular orbits.

4.1 Reliability of Our Numerical Simulations

We use the RKF7(8) integrator in our simulations. To investigate its validity, we check the conservation quantities E and $|\boldsymbol{J}|$, with $m/r = 1/100$ and $1/1000$ in one spin or two spins conditions, respectively. Figure 2 shows the relative errors of E and $|\boldsymbol{J}|$ without gravitational radiation. In the top panel, there is just one spin in that system, and the small parameter m/r is $1/100$. During the integration time span $25\,000\,T_0$, (T_0 the initial orbital period), i.e. $T_0 = 2\pi m^{-1/2} a_0^{3/2}$, $\Delta E/E$ and $\Delta|\boldsymbol{J}|/|\boldsymbol{J}|$ are confined to within 10^{-5} and 10^{-6}, respectively. In the bottom panel, two spins are taken account, and $\Delta E/E$ and $\Delta|\boldsymbol{J}|/|\boldsymbol{J}|$ both vary rapidly around 10^{-5}. Figure 3 is similar to Figure 2, but for $m/r = 1/1000$, in which $\Delta E/E$ varies between $10^{-8} - 10^{-7}$ with one spin and around 10^{-7} with two spins, and the corresponding ranges of

$\Delta|\boldsymbol{J}|/|\boldsymbol{J}|$ are $10^{-10} - 10^{-9}$ and $10^{-7} - 10^{-6}$. The step size we adopt in our integration is $T_0/100$. We would like to underline that the relativistic correction in Figure 3 is one whole magnitude smaller than that in Figure 2, and this is the main factor when explaining the difference between the two figures. In principle, relative errors of conservative quantities vary periodically within a specific range according to theoretical prediction, and the conservation laws held well in our numerical simulation, so our numerical integration is valid for these systems in the given time span.

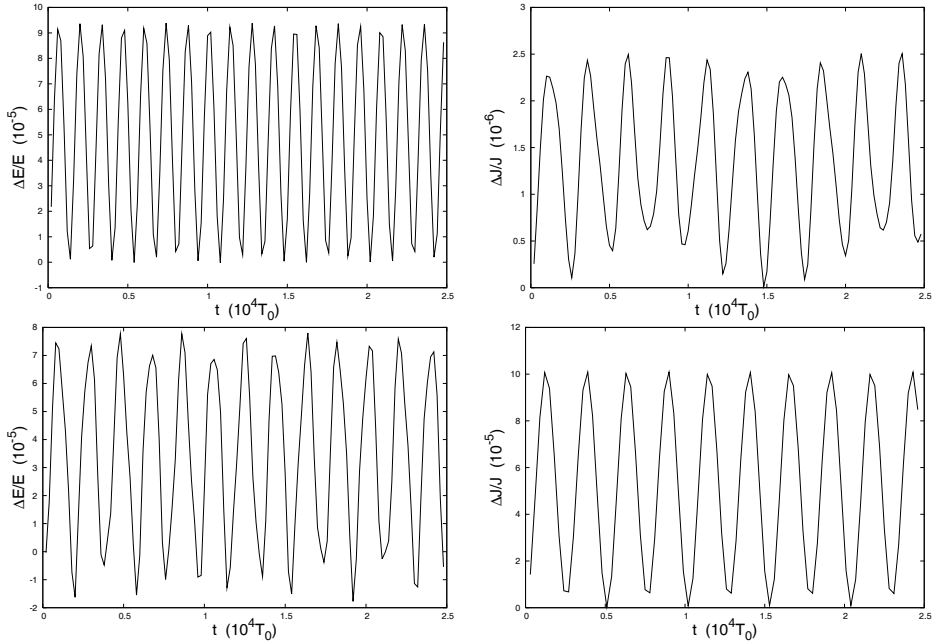

Fig. 2 Evolution of the relative errors of E and $|\boldsymbol{J}|$ in the case of no gravitational radiation. The unit of t is T_0 and the time span is $T = 25\,000\,T_0$. The initial conditions of the top panel are $\beta \equiv m_2/m_1 = 1/3$, $m/r = 1/100$, $x/m = 100$, $\dot{x} = 0$, $y = 0$, $\dot{y} = 0.1$, $S_1 = 0.65m_1^2$, $\theta_1 = 45^\circ$ and $S_2 = 0$. The initial conditions of the bottom panel are $\beta \equiv m_2/m_1 = 1/3$, $m/r = 1/100$, $x/m = 100$, $\dot{x} = 0$, $y = 0$, $\dot{y} = 0.1$, $S_i = 0.65m_i^2$, $\theta_i = 45^\circ$ and $i = 1, 2$.

To verify our code of Laskar's FMA, we applied it to the standard map before our calculation on the binary systems. By a comparison between the graph of the structure of the phase space and the map of frequency diffusion, we found they are consistent, and we applied our code to the Keplerian 2-body problem. As an integrable system its frequency diffusion should be strictly zero. Our result matches the theoretical prediction within our machine precision for sampling time span $T = 600\,T_0$.

4.2 Frequency Diffusion Map

To investigate the effects of spins, we make frequency diffusion map σ in the (θ_1, θ_2)- plane, θ_1, θ_2 being the angles between the spins and the orbital angular momentum at the initial instant. As a chaos indicator for a conservative system, the sign of σ could be ignored, so our frequency diffusion maps below portray just the absolute value of σ, when gravitational radiation is turned off. What concerns are: (1) the influence of using different sampling time span T on the diffusion map, (2) the effect of gravitational radiation reaction and (3) the influence of different mass ratios.

4.2.1 Sampling time span T

It has been shown that the accuracy of the FMA increases with increasing sampling time span T. Therefore, we pick up different sampling time span T in making frequency diffusion map.

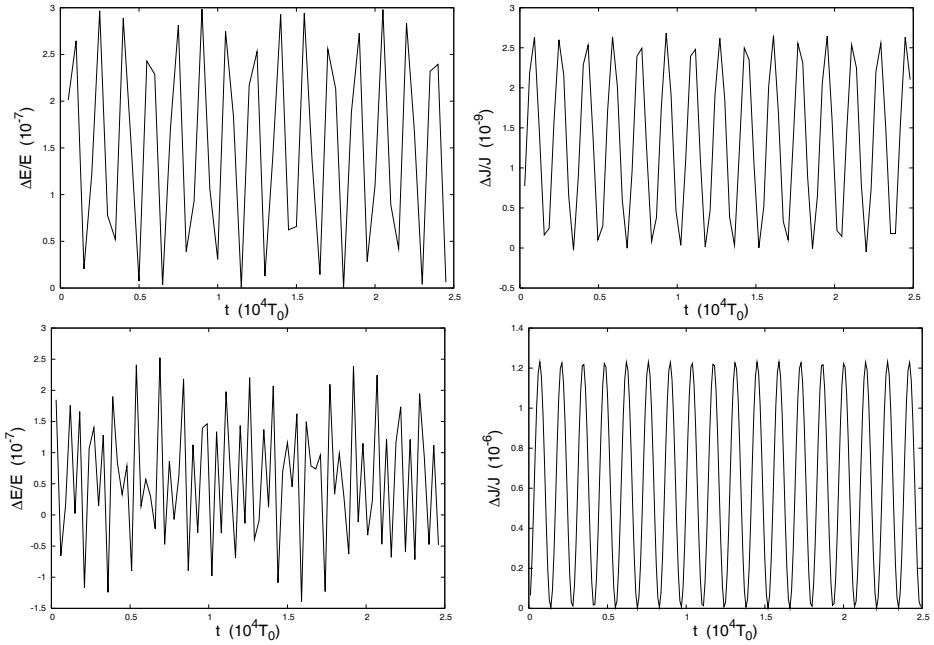

Fig. 3 Evolution of the relative errors of E and $|\boldsymbol{J}|$ in the case of no gravitational radiation. The unit of t is T_0 and the time span is $T = 25\,000\,T_0$. The initial conditions of the top panel are $\beta \equiv m_2/m_1 = 1/3$, $m/r = 1/1000$, $x/m = 1000$, $\dot{x} = 0$, $y = 0$, $\dot{y} = 0.0316$, $S_1 = 0.65m_1^2$, $\theta_1 = 45^\circ$ and $S_2 = 0$. The initial conditions of the bottom panel are $\beta \equiv m_2/m_1 = 1/3$, $m/r = 1/1000$, $x/m = 1000$, $\dot{x} = 0$, $y = 0$, $\dot{y} = 0.0316$, $S_i = 0.65m_i^2$, $\theta_i = 45^\circ$ and $i = 1, 2$.

Figure 4 shows the frequency diffusion map $|\sigma|$ of the orbit on grey scale in the (θ_1, θ_2)-plane, for different values of sampling time span T. The gray scale shown on the right of each map gives a quantitative measure of the chaotic indicator $|\sigma|$, brighter shades corresponding to more chaotic motion. In these cases, we neglect gravitational radiation. The only difference between the top and bottom panels is the sampling time span T ($T = 60\,T_0$ for the top, $T = 600\,T_0$ for the bottom). Obviously, the longer sampling time span gives more details. The reason is that $\nu_1 - \nu_1^T$ decreases as $T^{-(2p+2)}$ (see Eq. (11)). In our case $p = 1$, when the sampling time increases by a factor of 10, the precision of extracting frequency would increase by 10^4 and the frequency diffusion would be improved by 4 orders of magnitude. So we adopt $T = 600\,T_0$ in the following simulations.

Though they are made with different sampling time, these frequency diffusion maps have same high diffusion regions in both panels. These regions are all located at $\theta_1 \approx \pi/2$, which means chaos could be triggered off when $\boldsymbol{S}_1$ (the spin of the more massive component star) is perpendicular to the orbital angular momentum at the initial moment.

4.2.2 Gravitational radiation reaction

Gravitational radiation reaction (2.5 PN) is a dissipative factor in compact binaries, which causes decay of the orbits. In dynamics, it will break the torus in the phase space. That will violate the assumption of the FMA, the quasiperiodic approximation. Hence, the frequency diffusion map will be distorted inevitably.

Figure 5 shows the frequency diffusion σ of orbit on grey scale in the (θ_1, θ_2)-plane with gravitational radiation. Gravitational radiation would cause decay of the orbit, so we keep the sign of σ. As we can see, the diffusion maps are just distorted mildly or slightly when the sampling time span is short or the separation of two components is large, such as in the top panel and the bottom-right figure, but in the case of long sampling span and close components, gravitational radiation destroys the structure of diffusion map, such as in the bottom-left figure. The non-continuous belts in the top-left figure for $m/r = 1/100$ and

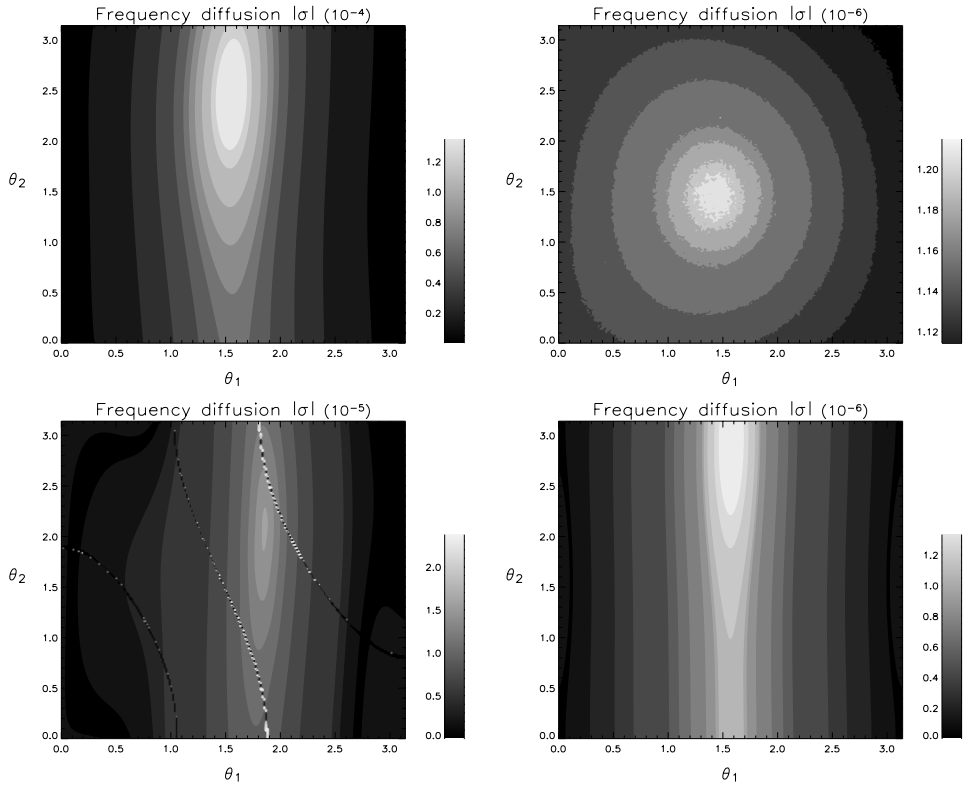

Fig. 4 Frequency diffusion map $|\sigma|$ of orbit in the (θ_1, θ_2)-plane for different sampling time spans T. Here we turn off the gravitational radiation. In the top panel $T = 60\,T_0$. The parameters in the left panel are $\beta \equiv m_2/m_1 = 1/3$, $m/r = 1/100$, and the initial conditions are $x/m = 100$, $\dot{x} = 0$, $y = 0$, $\dot{y} = 0.1$ and $\chi_1 = \chi_2 = 0.65$. The parameters in the right panel are $\beta \equiv m_2/m_1 = 1/3$, $m/r = 1/1000$, and the initial conditions are $x/m = 1000$, $\dot{x} = 0$, $y = 0$, $\dot{y} = 0.0316$ and $\chi_1 = \chi_2 = 0.65$. The bottom panel is similar to the top, but for $T = 600\,T_0$.

bottom-right figure for $m/r = 1/1000$ are caused by gravitational radiation dissipation. With increasing time span, these belts will develop and cover the whole figure, as in the bottom-left figure.

Due to the gravitational radiation (Brumberg 1991),

$$\frac{\mathrm{d}a}{\mathrm{d}t} = -\frac{64}{5}\frac{m_1 m_2 m}{a^3(1-e^2)^{7/2}}\left(1 + \frac{73}{24}e^2 + \frac{37}{96}e^4\right), \tag{14}$$

we have

$$n_k = m^{-1}\left[p^4 - \frac{512}{5}\frac{\beta}{(1+\beta)^2}\pi p^{3/2}k\right]^{-3/8}, \tag{15}$$

for quasicircular orbits at kth T_0, where a and e are the semi-major axis and eccentricity of the orbit, respectively. Here, $a_0 = a(0) = pm$, and $T_0 = 2\pi m p^{3/2}$. Assuming the decay of a causes mainly change in the fundamental frequency, we estimate

$$\sigma_k = 1 - \frac{\sum_{i=k+1}^{2k} n_i}{\sum_{i=1}^{k} n_i}, \tag{16}$$

in the short time approximation. We compare the results by the simulations and by analytic estimation (see Table 1) for the case of $\beta = 1/3$. In Table 1 $\bar{\sigma}_o$ is the average of σ from the simulations. It is shown that analytic estimations match our simulations. This means σ can represent most of the decay.

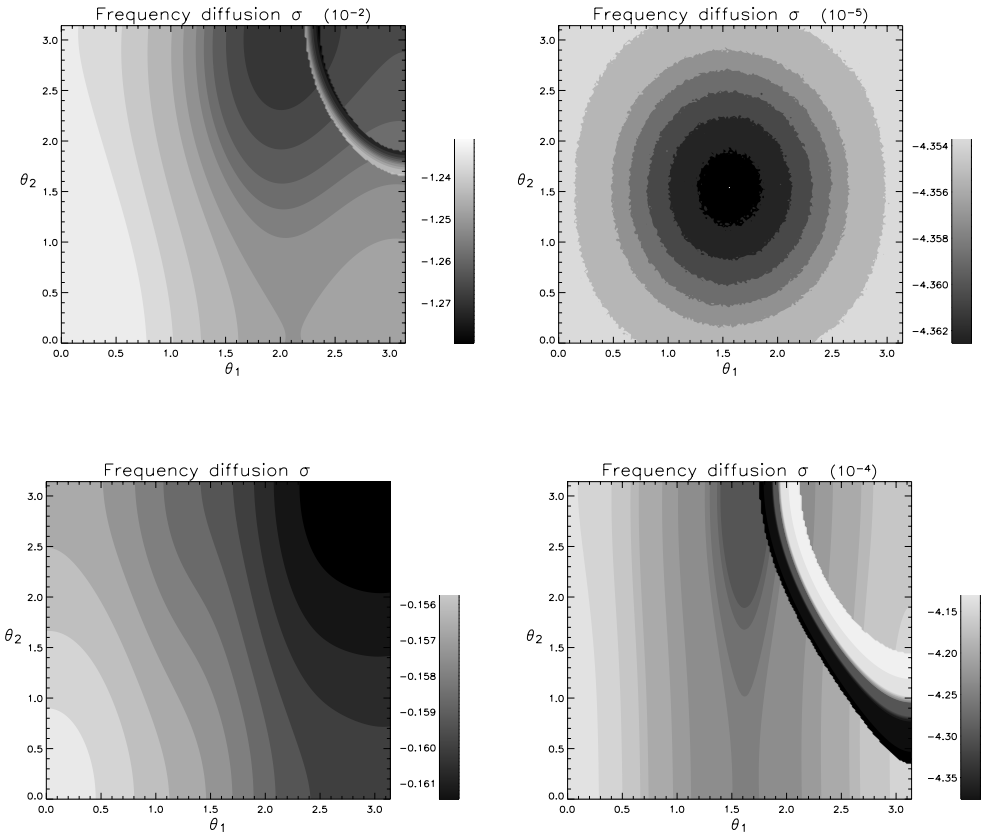

Fig. 5 All the conditions are the same as in Figure 4, except gravitational radiation reaction is turned on and the sign of σ is kept.

Table 1 Comparison of the Results by Numerical Simulations and Analytic Estimations

T	p	$\bar{\sigma}_o$	σ_k
$60\,T_0$	100	-1.25×10^{-2}	-1.42×10^{-2}
$60\,T_0$	1000	-4.35×10^{-5}	-4.29×10^{-5}
$600\,T_0$	100	-1.58×10^{-1}	-2.57×10^{-1}
$600\,T_0$	1000	-4.25×10^{-4}	-4.30×10^{-4}

In conclusion, gravitational radiation reaction will distort the frequency diffusion map when the sampling time span is short, and with increasing time span, it will dominate the map. In that case, the frequency analysis is no longer suitable as a chaos indicator, and the computed frequency diffusion represents mainly the decay of the orbit.

4.3 Mass Ratio

We investigate several cases with different mass ratios (see Fig. 6). All panels have identical initial conditions except the mass ratios, which are $\beta = 1$, $3/4$ and $1/2$ from the top row to the bottom. Here we are only concerned with the cases without gravitational radiation. In the case $\beta = 1$ ($m_1 = m_2$ and $S_1 = S_2$), it is natural that the map is symmetric about the line $\theta_2 = \theta_1$. However, high diffusion points are located in the region where the two spins nearly cancel each other. This is different from Hartl & Buonanno (2005), who found that initial nearly anti-alignment between the spins and the orbital angular momentum $\boldsymbol{L}$ trig-

gers off chaos. In the case of $\beta = 1/2$, the diffusion map is similar to previous map with $\beta = 1/3$, and the high diffusion region is concentrated around $\theta_1 \approx \pi/2$. The structure of the diffusion map with $\beta = 3/4$ is between the $\beta = 1$ map and $\beta = 1/2$ map, like some kind of transition. In addition, there are some non-continuous curves consisting of very low diffusion arcs (black) and very high diffusion dots (white) in the maps. These features emerge only after increase in the sampling time span. They deserve to study further in detail with intensive integration and LCE. In conclusion, different mass ratios have different initial conditions for chaos, and high diffusion region is just a tiny part in the whole diffusion map, which means chaotic orbits are few. Also, the values of σ suggest the chaos in the inspiral phase is weak.

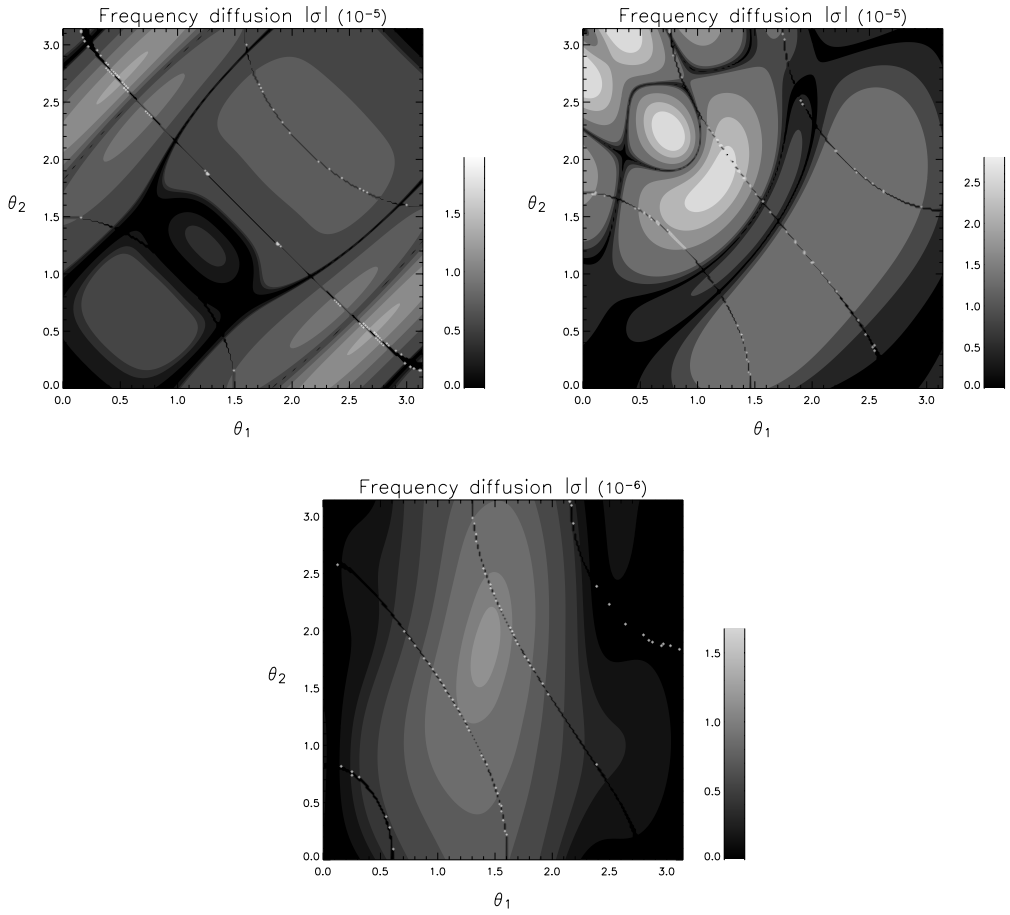

Fig. 6 Frequency diffusion of orbit in the (θ_1, θ_2)-plane with different mass ratios. The parameters common to the all panels are $m/r = 1/100$, sampling time span $T = 600\,T_0$. The initial conditions are $x/m = 100$, $\dot{x} = 0$, $y = 0$, $\dot{y} = 0.1$, $\chi_1 = \chi_2 = 0.65$. The mass ratios of the rows are $\beta = 1$, $3/4$ and $1/2$ from top down.

4.4 The Time of Arrival

Changing of the orbital configuration due to spins will modulate the time of arrival (TOA) of pulses if either or both components of the binary are pulsars. Chaos in orbital motion would cause abnormal changes of the time of arrival of pulses. Figure 7 shows the large difference in orbit configuration with the same parameters and initial conditions as before, except the angles between the spins and orbital angular momentum. The left panel shows the case of $\theta_i = 90^\circ$ which means both $\boldsymbol{S}_1$ and $\boldsymbol{S}_2$ are perpendicular to the orbital angular momentum; the right panel shows the case of $\theta_1 = 0^\circ$ and $\theta_2 = 90^\circ$ which means $\boldsymbol{S}_1$ is parallel to, and $\boldsymbol{S}_2$

is perpendicular to, the orbital angular momentum. We find that the value of z reached in the former case is larger than in the latter by a factor of 10. Figures 8 and 9 show when the line of sight is along the z axis (face-on), the frequencies of changing of inclinations and precession in those two cases are significantly different and the difference between the maximum delay in those two cases could be as large as a factor of 10. When the line of sight is along the x axis (edge on), the maximum delays of TOA are similar.

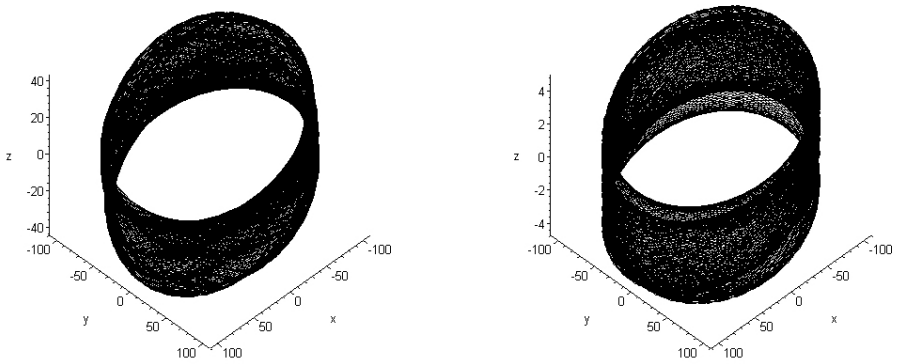

Fig. 7 Orbital configuration without gravitational radiation. Parameters: $\beta \equiv m_2/m_1 = 1/3$, $m/r = 1/100$ and $T = 260\,T_0$ for the integration time span. The initial conditions: $x/m = 100$, $\dot{x} = 0$, $y = 0$, $\dot{y} = 0.1$ and $\chi_1 = \chi_2 = 0.65$. Left: $\theta_1 = \theta_2 = 90^\circ$; right: $\theta_1 = 0^\circ$ and $\theta_2 = 90^\circ$.

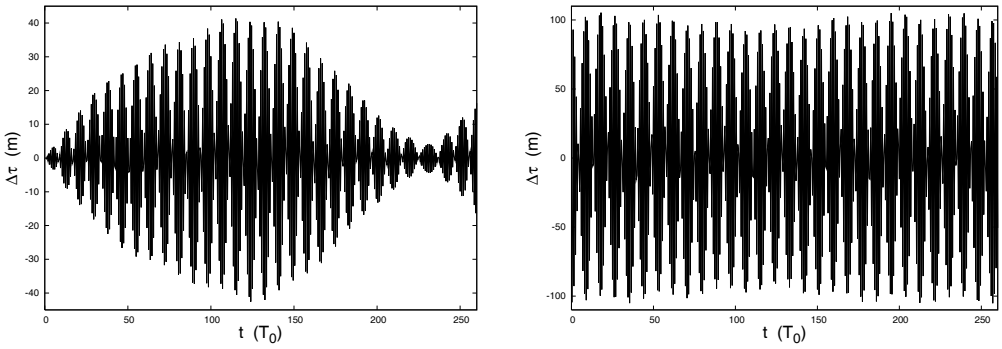

Fig. 8 Variation of time of arrival τ, without gravitational radiation. Parameters: $\beta \equiv m_2/m_1 = 1/3$, $m/r = 1/100$ and $T = 260\,T_0$ integration time span. The initial conditions: $x/m = 100$, $\dot{x} = 0$, $y = 0$, $\dot{y} = 0.1$, $\chi_1 = \chi_2 = 0.65$ and $\theta_1 = \theta_2 = 90^\circ$. Left: the line of sight is along the z axis (face-on); right: the line of sight along the x axis (edge-on).

5 CONCLUSIONS

Our numerical simulations with FMA show that spins play a critical role in the configuration of compact binaries. The mass ratio of the compact binary is also a really important factor for chaos. When the spins of the two components of an equal-mass binary nearly cancel each other ($\beta \sim 1$), chaos in orbits occurs. On the other hand, when the spins are perpendicular to the orbital angular momentum, the frequency diffusion of orbit will become remarkable for other comparable-mass systems ($\beta \sim 1/2$), which means the systems are irregular even chaotic, but based on our simulation, chaotic orbits are few and the chaos is weak for inspiral systems. Furthermore, a misalignment between the spins and orbital momentum will modulate the time of arrival of pulses if there is a pulsar in the binary, which depends sensitively on the direction of the

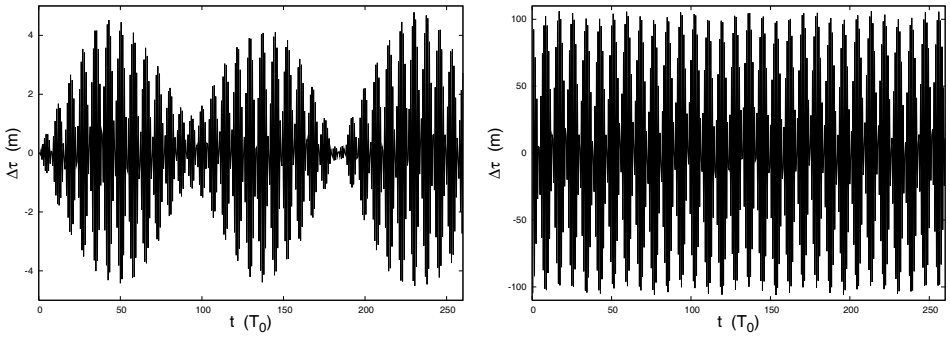

Fig. 9 Variation of time of arrival τ without gravitational radiation. Parameters: $\beta \equiv m_2/m_1 = 1/3$, $m/r = 1/100$ and $T = 260\,T_0$ for integration time span. Initial condition: $x/m = 100$, $\dot{x} = 0$, $y = 0$, $\dot{y} = 0.1$, $\chi_1 = \chi_2 = 0.65$, $\theta_1 = 0^\circ$ and $\theta_2 = 90^\circ$. Left: the line of sight is along the z axis; right: the line of sight along the x axis.

line of sight. Our work has proven that FMA is an efficient tool for investigating dynamical systems, but it cannot work as a perfect chaos indicator for compact binaries in their final stages, because of the existence of gravitational radiation and the failure of post-Newtonian approximation.

Acknowledgements We are grateful to an anonymous referee whose comments are very helpful to the final version of this article. We thank Dr. Peng-Fei Chen and Dr. Xiao-Yan Xu of Nanjing University for their help in data visualization, and Dr. Bi-Ping Gong for his helpful discussion and advices. This work was funded by the Natural Science Foundation of China (NSFC) under Grants 10233020 and 10563001.

References

Barker B. M., O'Connell R. F., 1975, Phys. Rev. D, 12, 329
Bombelli L., Calzetta E., 1992, Class. Quantum Grav., 9, 2573
Brumberg V. A., 1991, Essential Relativisticc Celestial Mechanics, Adam Hilger
Cornish N. J., Levin J., 2003, Phys. Rev. D, 68, 024004
Dettmann C. P., Frankel N. E., Cornish N. J., 1994, Phys. Rev. D, 50, R618
Hartl M. D., 2003, Phys. Rev. D, 67, 024005
Hartl M. D., 2003, Phys. Rev. D, 67, 104023
Hartl M. D., Buonanno A., 2005, Phys. Rev. D, 71, 024027
Karas V., Vokrouhlicky D., 1992, Gen. Relativ. Gravit., 24, 729
Kidder L., 1995, Phys. Rev. D, 52, 821
Kramer M., 2004, preprint (astro-ph/0409020)
Laskar J., 1990, Icarus, 88, 266
Laskar J., 1993, Physica D, 67, 257
Laskar J., Froeschlé C., Celletti A., 1992, Physica D, 56, 253
Levin J., 2000, Phys. Rev. Lett., 84, 3515
Levin J., 2003, Phys. Rev. D, 67, 044013
Robutel P., Laskar J., 2001, Icarus, 152, 4
Schnittman J. D., Rasio F. A., 2001, Phys. Rev. Lett, 87, 121101
Suzuki S., Maeda K., 1997, Phys. Rev. D, 55, 4848
Varvoglis H., Papadopoulos D., 1992, A&A, 261, 664
Wu X., Huang T.-Y., 2003, Phys. Lett. A, 313, 77
Wu X., Huang T.-Y., Zhang H., 2006, Phys. Rev. D, 74, 083001
Wu X., Zhang H., 2006, ApJ, 652, 1466